Received: 24 February 2023 | Revised: 25 June 2023 | Accepted: 19 July 2023

DOI: 10.1002/jbio.202300063

RESEARCH ARTICLE

JOURNAL OF BIOPHOTONICS

Skin-color-independent robust assessment of capillary refill time

Raquel P. de Souza Bachour | **Eduardo Lopes Dias** | **George C. Cardoso**

Department of Physics, FFCLRP, University of São Paulo, São Paulo, Brazil

Correspondence
Raquel P. de Souza Bachour, Department of Physics, FFCLRP, University of São Paulo, São Paulo 14040-901, Brazil.
Email: raquel.pantojo.souza@usp.br

Funding information
Coordenação de Aperfeiçoamento de Pessoal de Nível Superior

Abstract

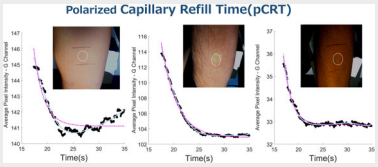

Capillary Refill Time (CRT) assesses peripheral perfusion in resource-limited settings. However, the repeatability and reproducibility of CRT measurements are limited for individuals with darker skin. This paper presents quantitative CRT measurements demonstrating good performance and repeatability across all Fitzpatrick skin phototypes. The study involved 22 volunteers and utilized controlled compression at 7 kPa, an RGB video camera, and cocircular polarized white LED light. CRT was determined by calculating the time constant of an exponential regression applied to the mean pixel intensity of the green (G) channel. An adaptive algorithm identifies the optimal regression region for noise reduction, and flags inappropriate readings. The results indicate that 80% of the CRT readings fell within a 20% range of the expected CRT value. The repetition standard deviation was 17%. These findings suggest the potential for developing reliable and reproducible quantitative CRT methods for robust measurements in patient triage, monitoring, and telehealth applications.

KEYWORDS
capillary refill time, non-invasive monitoring, peripheral perfusion

1 | INTRODUCTION

Capillary refill time (CRT) is one of the most widely acknowledged and used methods [1, 2] to estimate peripheral perfusion status [3–5], for quick assessment or in low-resource environments. CRT is defined as the time it takes for a distal capillary bed to regain its normal color after having received enough mechanical compression to cause blanching [6] of the skin surface. Compression is typically applied by the finger of the person who measures, who uses a chronometer and their own visual assessment to measure the refill time [7–9]. CRT measurement sites in humans include the sternum [10], the forearm [11], the legs and feet [9, 12, 13], the fingertips [14, 15], and the knees [16, 17]. When performed in ideal conditions by trained professionals, CRT has been used to diagnose septic shock [18], dehydration in children [3, 19, 20], and viral diseases, such as dengue [21], and, more recently, as a prognostic factor in patients with COVID-19 [22].

Among CRT's main advantages are simple equipment, high speed, and simplicity in training. Yet, the adoption of CRT is hampered by concerns about its inter- and intraobserver reproducibility, a lack of standardization for pressure and duration of compression [4, 6, 23, 24], the effect of external factors such as the lighting in the room [25] and the temperature of the limb and the environment [6, 12, 26], and the effect of skin color, particularly dark skin, on CRT accuracy [17, 27]. These limitations have called into question the applicability and usefulness of manual CRT measurements [6, 18, 28]. Attempts

to improve the reliability and objectivity of CRT measurements include the proposal of a device that utilizes optical assessment of diffuse reflectance on the skin to calculate the CRT [11], a device comprising a compressible plastic optical fiber to measure CRT under the foot [13], and a video camera system for training personnel to perform traditional CRT measurements [29].

Video-based CRT measurements [23, 30–33] have been proposed due to the higher sensitivity and linearity of RGB cameras compared to the human eye. Cameras allow for the detection of subtle hues and intensity changes between the time of skin compression and its capillary refilling to the original state. While some studies simply visually analyze the CRT videos at a later time [33], others automate video processing [31]. Shinozaki et al. [23] acquire the RGB channels' intensities during a fingertip test, fit an exponential decay between the instants of maximum compression and 90% recovery and obtain CRT with success. We could not find studies in the literature addressing issues such as CRT uncertainties, reproducibility, reliability, and robustness with respect to skin phototypes. In addition, the literature lacks studies of CRT under controlled conditions.

In the present paper, we show that CRT can be made robust and reliable, at least by using controlled compression, video processing, and polarized light. By robust, we mean insensitive to perturbations such as measurement repetitions and measurement reproductions with changes in skin phototypes. By reliable, we mean that inadequate or poor measurements are identified and flagged to be repeated. Our method is based on recording a video of a region of interest (ROI) after the release of the compression. It uses image processing and curve fitting to calculate the CRT, and cocircular polarizers between the light source and the camera to attenuate the light reflected on the outer surface of the skin. We tested our method on 22 volunteers, including all Fitzpatrick phototypes, under controlled conditions of temperature, lighting, and applied pressure.

To distinguish our CRT method from other studies in the literature, we name it polarized CRT (*pCRT*). The polarized light is not essential but is known to increase robustness in skin measurements. This terminology will be adopted for the remainder of the paper.

2 | MATERIALS AND METHODS

2.1 | Study subjects

We chose to invite volunteers that represented all Fitzpatrick skin types and aged above 20 years. Twenty-two healthy volunteers (aged 20–70 years; 9 female), comprising all Fitzpatrick skin types (I–II; III–IV, and V–VI) chose to participate in this study after being detailed about the procedure (University of São Paulo Ethics Committee CAAE 95342518.1.0000.5407, 3.046.098 FFCLRP).

2.2 | Experimental protocol

We have built a cylindrical compression device to produce skin blanching on the volunteer's forearm (Figure 1A). The cylindrical device (Aluminum) smoothly slid inside a hollow external acrylic cylindrical vest to gently rest on the volunteer's forearm. To thermally insulate the metallic cylinder from the skin, it was capped with a circular Teflon cap (4 cm^2) featuring rounded corners. The rounded corners' radius was sufficient to prevent pressure marks on the skin.

An LED light source (E27, TKL-90 model, 14 W, Taschibra Ltda, Brazil) was used to illuminate the forearm. As a precautionary measure for experimental reproducibility in this study, the light source was activated at least 15 min prior to each data acquisition to avoid potential warm-up transient effects.

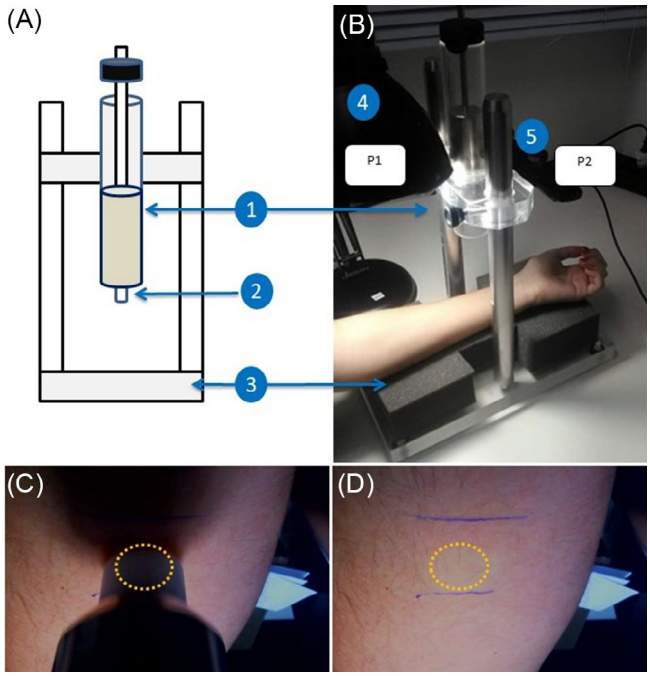

FIGURE 1 Experimental setup. (A) Schematic illustration of the weight and arm support, front view; (1) Standard aluminum cylindrical weight; (2) thermally insulating Teflon cap ($4cm^2$), that comes into contact with the subject's skin; (3) Armrest (dense polyurethane foam). (B) Setup with a volunteer's arm in actual measurement position; (4) light source and (5) video camera, with cocircular polarizers (P1 and P2) installed. (C) Weight lowered on a volunteer's forearm as viewed by the video acquisition camera. The ROI is highlighted by the dotted circle. (D) Blanching of the ROI after the release of compression.

The video camera was recorded at 30 frames per seconds (HD Pro-C525, 1280 × 720 pixels, video container: WMV, encoding: YUV12; Logitech S.A., Switzerland) and the light source was attached to a fixture (Figure 1B). The camera was focused on each subject's region of interest (ROI) on the forearm, 9 cm from the wrist line. To block specular reflections [34, 35], cocircular detection [36] was used. Circular polarizers ($\lambda/4 = 125$ nm, 99.98% polarization efficiency, crossed transmission 0.5%, 3D Lens Corp., Taiwan ROC) were placed both in front of the light source and camera lens, with their quarter-wave plate sides facing the forearm (P1 and P2 in Figure 1B).

The experiments were performed in a temperature-controlled room (20°C – 22°C) as suggested by Pickard et al. [6]. All videos were acquired in a dark room illuminated only by the circularly polarized light source. Before the start of the measurements, the volunteers remained seated for 10 minutes for acclimatization. The volunteers sat in a relaxed position on a height-adjustable chair with their left arm positioned approximately at the heart level (Figure 1B). For each measurement, the camera started recording the ROI for 10 s before the weight was lowered on the subject's left forearm, where it remained for 5 s applying a pressure of 7 kPa, after which it was lifted for recording the capillary refill. The recording was stopped 20 s after the lifting of the weight, which is much longer than the capillary refill times. These pCRT readings were repeated five times for each subject, with a 1-minute rest between readings. The WMV video files were processed offline at a later time.

2.3 | Video analysis and pCRT calculation

The placement and subsequent removal of the cylindrical weight from the skin surface result in a pronounced color alteration. The average intensities of the R, G, and B channels of the ROI pixels are calculated for each frame (Figure 2A) and the G-channel (Figure 2A) presents the best signal-to-noise ratio. We hypothesized that the behavior of the G-channel decay during CRT can be modeled by an exponential decay. However, a single-exponential decay model quickly fails after a few time constants: the decay time constant changes and/or intensities become noisy (see Figure 2A). Thus, we have devised a multistep protocol to realize the exponential regression.

First, we identified a cutoff time t_c, after which the exponential decay model significantly diverges from the observed curve. To find t_c, we simultaneously fit a 6th-order polynomial and a provisional exponential decay on the entire G channel intensity curve, after the release of the compression. The 6th-order polynomial is a compromise between accommodating up to three oscillations in the data, and still serving as a low-pass filter for the data. The point of maximum divergence between the polynomial and the provisional exponential identifies t_c (Figure 2B and Figure 3A). This procedure proved to be robust for all our instances. Finally, pCRT is the time constant of yet another exponential decay function:

$$I = I_o \exp\left(-\frac{t}{pCRT}\right) \quad (1)$$

fitted to the original data within the interval between the position of the maximum value of the G-channel and t_c (inset of Figure 2B). A pCRT *reading* is obtained from the regression, where the 95% confidence interval (CI) is $pCRT \pm \sigma_{95\%CI}$. This uncertainty is not the pCRT uncertainty, but the uncertainty in the regression in one reading. The actual pCRT uncertainty is larger than $\sigma_{95\%CI}$ and can only be estimated by multiple readings of pCRT. In Equation (1), the offsets in time and in intensity have been omitted for simplicity. Details can be found in the code made available in the supplementary material online (https://github.com/Photobiomedical-Instrumentation-Group/pCRTMatlab). The procedure described in this paragraph was applied to every acquired video.

We analyzed all 110 video files (5 for each of the 22 volunteers) with scripts we specially developed for pCRT determination. The scripts were implemented in Matlab version 2015a (MathWorks, MA, USA).

2.4 | Statistics and repeatability test

We adopted relative uncertainty $\sigma_{95\%CI}/pCRT$, as the primary metric to assess the quality of each pCRT reading. The repeatability test of pCRT was evaluated by analyzing the distribution of five readings from each volunteer, from phototype groups, and for all subjects together. We also established a maximum acceptable value of the relative uncertainty for a single measurement, which we call the *discard-and-repeat* threshold, to flag and remove readings likely to be incorrect while keeping plausible ones. The analysis of the results involved descriptive statistics to summarize the data, as well as ANCOVA to account for confounding variables.

3 | RESULTS

In healthy tissue, after the skin is bleached out by compression, the color returns rapidly as the blood refills the dermal capillaries. This color return is the foundation of

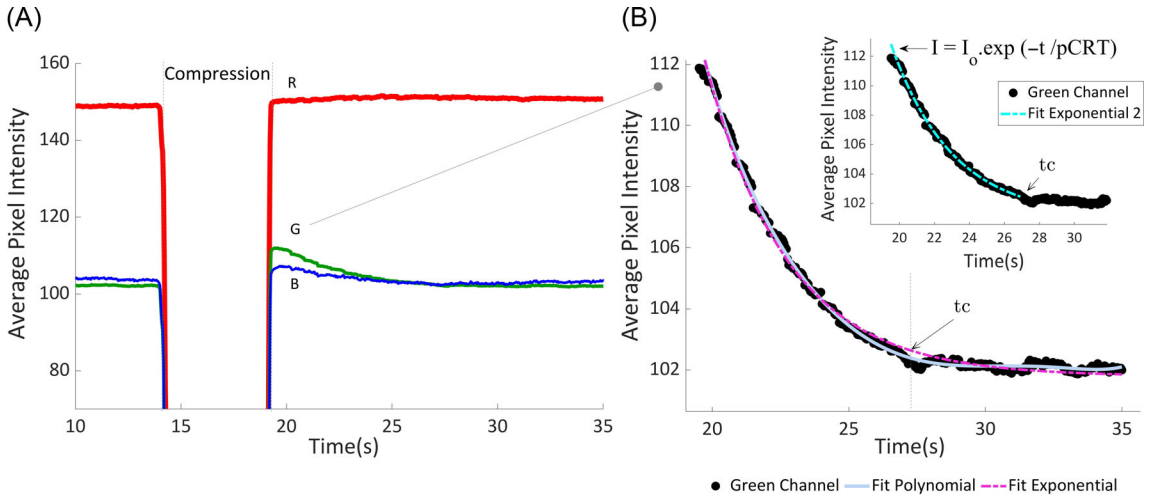

FIGURE 2 Mean ROI pixel intensities during a pCRT experiment (for a volunteer of phototype III–IV). (A) Mean intensities of the R, G, and B channels from the pixels inside the ROI. The cylindrical weight blocking the camera during compression causes a sharp drop in intensities observed between 14 and 19 s. After the weight is lifted, the G-channel displays a pronounced peak and a decay, which is highlighted in (A) Behavior of the G-channel after the compression is lifted. The decay is approximately exponential but levels off after the *cutoff time* (t_c); the inset shows the exponential regression only up to t_c, used to determine pCRT.

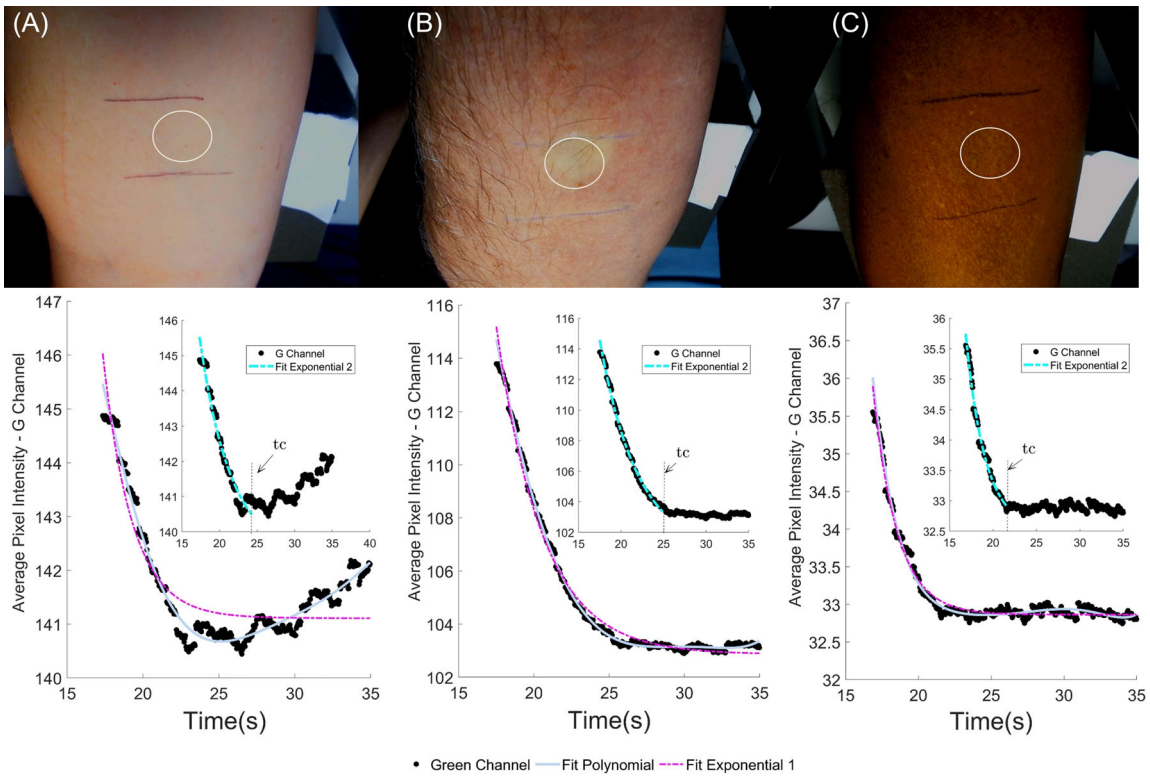

FIGURE 3 Forearms of different phototypes immediately after removal of the 7 kPa compression on the ROI (circle). (A) Phototype I–II, (B) Phototype III–IV, and (C) Phototype V–VI. The corresponding G-channel mean ROI intensity decay and curve regressions are shown below each volunteer image. Note that curve behavior is not exponential for times longer than t_c.

the CRT test. Our pCRT method calculates capillary refill time by analyzing the ROI's image intensity over time. As shown in Figure 2, the exponential decay of intensity characteristic of capillary refill is most clearly distinguishable in the G-channel. The higher signal-to-noise (SNR) ratio of the G-channel held for all our measurements, across all subjects. Thus, we chose to perform our analysis on the G-channel only.

Table 1 summarizes pCRT results for each skin phototype group. Because the age distributions are different for the different phototypes, we performed an ANCOVA analysis to compare the average pCRT values for the different phototypes controlled for the confounder age. We found the mean pCRT for the different phototypes, even after controlled for the confounder age, do not differ significantly (p value = 0.1528 ANCOVA). We also confirmed that pCRT has a small but significant dependency on age (p value = 0.0013 ANCOVA) as already reported in the literature [1, 37]. Due to the limited number of volunteers ($n = 22$), further investigation into the relationship between CRT and age is beyond the scope of our study. Our main result is that the independence of pCRT on phototype suggests its robustness with respect to light absorption by melanin.

Differences in the mean pCRT might stem from differences in the age groups and respective standard deviations, but the small number of volunteers in each group prevents further interpretation. Additionally, individual t-tests were conducted to compare the pCRT values among the phototype groups. The results indicated no statistically significant differences in pCRT between Phototypes I–II and Phototypes III–IV ($p = 0.815$), Phototypes I–II and Phototypes V–VI ($p = 0.7693$), or between Phototypes III–IV and Phototypes V–VI ($p = 0.788$). These findings suggest that there is no significant variation in pCRT across the different phototype groups.

Figure 4 shows the histogram of all pCRT readings. Figure 4A displays pCRT readings, with a mean of 3.9 s; Figure 4B displays the corresponding relative regression uncertainties $\sigma_{95\%CI}/pCRT$ with a median 7.1%. One measurement, with $\sigma_{95\%CI}/pCRT > 45\%$, was omitted.

Figure 5 displays the distribution of measurement uncertainties, providing a perspective of the pCRT results for all three phototype subgroups studied. Most pCRT readings exhibit a relative regression uncertainty 10%. Note, however, a prominent outlier with a relative regression uncertainty exceeding 45%, with a clearly incorrect pCRT estimate. To improve the reliability of results, we decided to flag and discard such outliers (discard-and-repeat threshold), by discarding readings with a relative regression uncertainty $\sigma_{95\%CI}/pCRT$ above 10%.

Figure 6 shows the results of the repeatability test. The vertical axis of Figure 6A represents individual pCRT readings normalized by the mean value ($\langle pCRT \rangle$) obtained from the five readings for each individual. The horizontal axis used box plots to compare $\sigma_{95\%CI}/pCRT$ for the whole set (110 readings) with data with suspected outliers that have been discarded by the $(\sigma_{95\%CI}/pCRT) > 10\%$ threshold (86 readings remaining). If repeatability were perfect, every reading would be identical to the average of the five readings: $pCRT/\langle pCRT \rangle = 1$ for any pCRT reading. Consequently, the relative error $\delta = |(pCRT/\langle pCRT \rangle) - 1|$ would be zero for all pCRT readings. However, we observed variability in the readings. For our data, $SD_{pCRT/\langle pCRT \rangle} = 30\%$ before use of the discard threshold,

TABLE 1 Mean pCRT for different Fitzpatrick skin types. pCRT differences between phototype groups were not statistically significant even after accounting for age as a confounder ($p = 0.1528$, ANCOVA).

Groups	pCRT ± SD (s)	Age ± SD (yr.)	Number of volunteers
Phototypes I–II	4.0 ± 0.7	27 ± 12	8
Phototypes III–IV	4.4 ± 1.3	46 ± 14	9
Phototypes V–VI	3.7 ± 1.7	44 ± 19	5

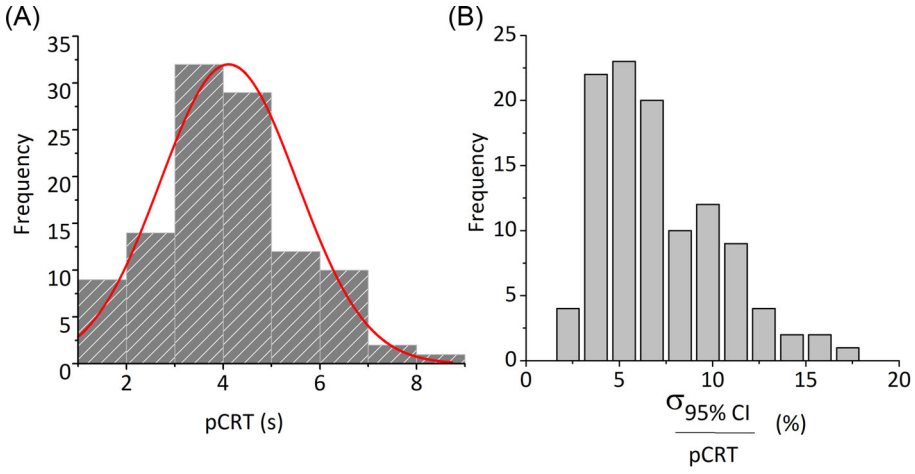

FIGURE 4 Descriptive statistics for all pCRT readings. (A) The distribution of pCRT results for all 110 data points (five readings for each volunteer). The red line is a Gaussian fit (mean = 3.9; SD = 1.3). (B) Frequency distribution of the coefficient of variation $\sigma_{95\%CI}/pCRT$ (median = 7.1%).

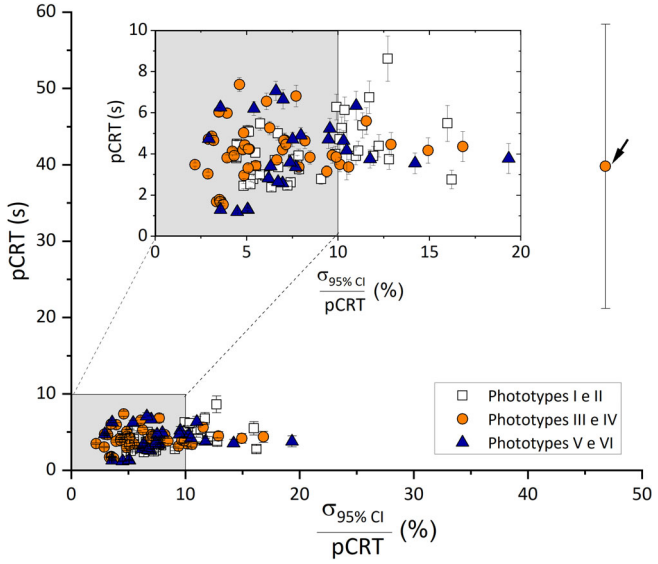

FIGURE 5 Distribution of pCRT readings for all phototype subgroups. All 110 readings are shown (5 for each of the 22 subjects). The error bars represent $\sigma_{95\%CI}$. The arrow highlights a point with abnormally high regression uncertainty, which indicates an erroneous measurement. The gray box in the inset shows the region with relative regression uncertainty below 10%, which is our reading's discard threshold. Note that all phototypes are approximately equally represented and evenly distributed inside the gray box.

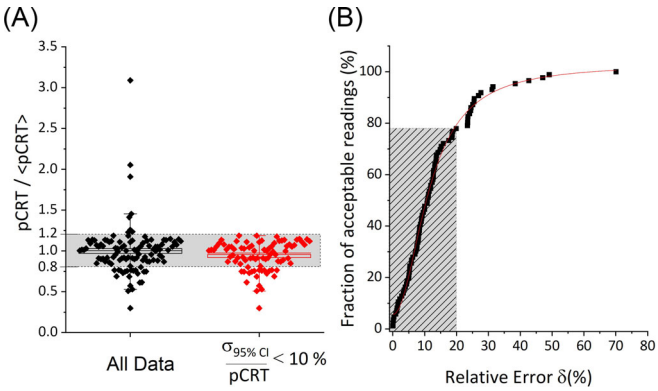

FIGURE 6 Repeatability analysis. (A) The vertical axis represents the ratio between each pCRT reading and the mean of 5 repetitions $\langle pCRT \rangle$. The box plots compare all readings (black diamonds, 110 points, $SD_{pCRT/\langle pCRT \rangle} = 30\%$), with readings remaining after application of a 10% discard-and-repeat threshold (red diamonds, 86 points $SD_{pCRT/\langle pCRT \rangle} = 17\%$). (B) Fraction of acceptable readings as a function of the relative error δ (difference between a given measurement and the average of the five readings). The grayed-out box illustrates a maximum acceptable error of $\delta = 20\%$, when the fraction of acceptable readings is 78%. The red line shows a logistic fit ($R^2 = 0.995$).

and $SD_{pCRT/\langle pCRT \rangle} = 17\%$ after application of the discard threshold. Thus, pCRT presents a SD of less than 20%, as the combined physiological and measurement variability.

Defining an acceptable reading as one that exhibits a lower than δ error relative to the average of five readings from an individual, the proportion of acceptable readings increases as the acceptable relative error δ increases (Figure 6B). By choosing a discard-and-repeat threshold of $\sigma_{95\%CI}/pCRT > 10\%$, approximately 80% of the original 110 readings remained. Among these retained readings, approximately 80% fell within the range of $\langle pCRT_i \rangle \pm 20\%$, where $\langle pCRT_i \rangle$ represents the average pCRT for the i-th subject (highlighted in gray in Figure 6B). If precision is relaxed to $\delta > 35\%$, approximately 95% of the non-discarded pCRT readings are acceptable (Figure 6B). The curve in Figure 6B is well-fitted by a logistic function ($R^2 = 0.995$), indicating that the relative error distribution remains largely Gaussian even after applying the discard threshold. A more stringent discard-and-repeat reading threshold ($\sigma_{95\%CI}/pCRT$ criterion) would flag and reject a greater number of pCRT readings. On the other hand, the proportion of acceptable readings for a given δ would increase, leading to a steeper rise of the curve illustrated in Figure 6B.

4 | DISCUSSION

We have shown that capillary refill time can be measured repeatedly and robustly, with low pressure applied to the skin. For that end, we used controlled pressure, cocircular polarized light imaging, and image processing. The use of cocircular polarizers [36] attenuates the reflection component of light captured by the digital camera, enabling visualization of deeper regions of the skin [36, 38]. Our system produced successful measurements in subjects with dark skin (phototypes V and VI), which are a challenge for visual CRT measuring methods [27, 39, 40], and has not been demonstrated by other studies. We are not aware of earlier studies that have successfully performed the CRT test in volunteers of all skin phototypes (Table 1).

For all volunteers studied, the G-channel average intensity presented an approximately exponential decay with a good signal-to-noise ratio (SNR) compared to the other channels. While the R-channel exhibited negligible CRT signal for all phototypes (Figure 2A is typical), The B channel displayed a clear pCRT signal for individuals with low melanin skin tones (Figure 2A, for example). However, for phototypes V–VI, the B channel either showed no pCRT signal or had poor SNR due to increased melanin absorption. In contrast, the G-channel consistently enabled pCRT readings with a good SNR regardless of the phototype. This can be attributed to a tradeoff between light absorption and scattering by the skin

(which varies based on melanin levels) and light absorption by hemoglobin [41].

We developed a flagging recipe to discard and repeat most poor readings. Thus, the chance of an erroneous reading is reduced at the cost of increasing the fraction of rejected readings. On observing the data, we chose readings with relative regression uncertainty lower than of 10% to be "acceptable readings." Note that the regression uncertainty pertains only to the regression method and is not the same thing as uncertainty or error in the pCRT reading. Out of the acceptable readings, 80% (CI 95%) had a relative error (δ) lower than $0.2\langle pCRT\rangle$ (Figure 6B).

The combined variability due to physiology and measurement method gives a SD = 30% without discarding readings, and SD = 17% when readings with relative regression uncertainty higher than 10% are discarded (Figure 6A). Averaging two or more readings can further decrease the fraction of readings with low relative error δ. In practice, a compromise must be made between discarding and repeating readings and risking a high relative error result.

The use of an exponential regression with a cutoff time contributes to the reproducibility of the pCRT results. After the end of the steep decay region of the curve, in some individuals the curve becomes noisy, and in other individuals, the exponential time constant may change (Figure 3, graphs below the images). We believe that these changes are caused by mechanical changes in elasticity of the skin, and by different time dynamics of subjacent fat and muscle, which also depend on the state of hydration of the tissue [42]. To stabilize the exponential regression, we established a cutoff time to limit the exponential fit to the region of steep fall of the curve, as detailed in Section 2.3. The cutoff strategy improves the quality of the exponential regressions and the repeatability of the readings. Except for the cutoff strategy, our regression method follows approximately the one proposed by Shinozaki et al. [30] that calculates CRT fitting and exponential decay to the gray scale video signal. They use a cutoff between 90% and 10% of the decay curve and do not take advantage of regression uncertainties.

Though pCRT relates to the same physiological parameters as CRT and yields value similar to the visual CRT measurement method [6, 43], they differ in values. The values for pCRT are larger than for visual CRT. The difference may be due to the lower pressure we apply (7 kPa) compared to conventional CRT [11, 30, 44, 45] and/or to the improved visibility of blood perfusion in the skin provided by cocircular polarized imaging. The compression applied to induce whitening of the ROI is one of the many factors known to influence CRT [26, 46]. Ordinarily, these compressions are subjective and are typically applied with the examiner's fingertip. Different researchers have proposed different compressions. For example, Kawaguchi et al. propose a pressure of 10 kPa - 70 kPa applied with the fingertip for 2 seconds as optimal [44]. Other studies have proposed 17 kPa [11, 45], and 60 kPa [30]. We have adopted throughout this study the lowest pressure yet, 7 kPa, which is low enough not to induce any pain in the forearm. With this low pressure, we demonstrated repeatability. In another study to be published elsewhere, we noticed that the application of high pressure in the forearm (23 kPa) increased noise, decreased fit quality, and repeatability. Our success with using low pressure (7 kPa) may be attributed not only to the higher sensitivity of digital cameras but also to the use of cocircular polarizers, which improves SNR by attenuating the component due to reflection on the skin surface [35, 36, 38]. We believe that with adequate image processing and illumination aimed to avoid reflections, the polarizers may be unnecessary.

We chose to assess CRT on the forearm instead of the fingertip for two main reasons. First, given the primary objective of our study, which focused on investigating the robustness of the technique, we recognized that the fingertip, due to its high susceptibility to peripheral temperature changes, could introduce additional variability into the results [23, 26]. The forearm provides a more stable baseline for our measurements. Second, by incorporating forearm assessments, we aimed to expand the existing body of literature on CRT studies, thereby advancing the overall understanding and practical application of this technique.

Limitations of this study include the utilization of data from a healthy group aged 20–70 years, thereby minimizing the confounding effects of disorders or diseases on the obtained results. However, as demonstrated by several previous studies, it is well-established that depending on the specific disease, pCRT values would deviate from the values found in a healthy control group [21, 22, 32, 47]. Another potential limitation involves the potential interference of the cardiovascular and parasympathetic systems in the volunteers during the five CRT readings. Volunteers may have found the experiment to be stressful or at least initially uncomfortable due in part to the cold, unlit environment, unfamiliar equipment, and the requirement to stay still during most of the process. This situation may have caused the activation of the sympathetic nervous system of some volunteers during data acquisition, which induces a change in the heart rate (HR) [1, 48]. Heart rate and temperature are factors known to influence CRT [49], this may have caused intra-participant pCRT variation along the 5 readings.

Other limitations of this study are the lack of skin temperature measurement, and the relatively small number of volunteers did not allow further investigations on pCRT dependence with multiple variables.

The robustness of different phototypes and the good repeatability of pCRT opens up the possibility for health condition status tracking and physiological monitoring studies where the conventional CRT method has proved unreliable. Among the possibilities that remain to be studied are the relationship between pCRT and temperature, heart rate, blood pressure, or with the autonomic nervous system.

5 | CONCLUSION

We have demonstrated that CRT can be made robust, independent of the observer and skin color, and can be performed at low compression using simple equipment. These findings hold promise for further research in a clinical setting and quantitative CRT. Further advancements in the method have the potential to reliably assess an individual's capillary refill time over time, facilitating effective tracking of health conditions.

SUPPLEMENTARY MATERIALS

The code used for this work is available at https://github.com/Photobiomedical-Instrumentation-Group/pCRTMatlab.

AUTHOR CONTRIBUTIONS

Conceptualization: Raquel P. de Souza Bachour, Eduardo Lopes Dias, and George C. Cardoso; Formal analysis: Raquel P. de Souza Bachour, Eduardo Lopes Dias, and George C. Cardoso; Methodology: Raquel P. de Souza Bachour; Software: Raquel P. de Souza Bachour; Supervision: George C. Cardoso; Validation, George C. Cardoso; Writing—original draft: Raquel P. de Souza Bachour; Writing—review and editing: Raquel P. de Souza Bachour, Eduardo Lopes Dias, and George C. Cardoso. All authors contributed to the article and approved the submitted version.

ACKNOWLEDGMENTS

The authors thank Beatriz Janke and Carlos Renato da Silva, for experimental help, and all the volunteers who participated in the experiment.

FUNDING INFORMATION

This study was financed by the Coordenação de Aperfeiçoamento de Pessoal de Nível Superior—Brazil (CAPES)—Finance Code 001.

CONFLICT OF INTEREST STATEMENT

The authors declare no conflicts of interest.

INFORMED CONSENT

Informed consent was obtained from all subjects involved in the study.

ORCID

Raquel P. de Souza Bachour https://orcid.org/0000-0002-1727-3326

REFERENCES

[1] D. L. Schriger, L. Baraff, *Ann Emerg Med* **1988**, *17*, 932.
[2] D. A. Osborn, N. Evans, M. Kluckow, *Arch Dis Child Fetal Neonatal Ed* **2004**, *89*, 168F.
[3] A. Lima, T. C. Jansen, J. Van Bommel, C. Ince, J. Bakker, *Crit Care Med* **2009**, *37*, 934.
[4] E. D. V. Espinoza, S. Welsh, A. Dubin, *Rev Bras Ter Intensiva* **2014**, *26*, 269.
[5] D. King, R. Morton, C. Bevan, *Arch Dis Child Educ Pract Ed* **2014**, *99*, 111.
[6] A. Pickard, W. Karlen, J. Mark Ansermino, *Anesth Analg* **2011**, *113*, 120.
[7] ADAM Watson and Anne-Maree Kelly, *Emerg Med* **1993**, *5*, 90.
[8] N. Venkata Raju, M. Jeffrey Maisels, E. Kring, L. Schwarz-Warner, *Clin Pediatr* **1999**, *38*, 139.
[9] E. Bridges, *Am J Nurs* **2017**, *117*, 34.
[10] J. Crook, R. M. Taylor, *Arch Dis Child* **2013**, *98*, 265.
[11] L. L. Blaxter, D. E. Morris, J. A. Crowe, C. Henry, S. Hill, D. Sharkey, H. Vyas, B. R. Hayes-Gill, *Physiol Meas* **2015**, *37*, 83.
[12] M. H. Gorelick, K. N. Shaw, M. D. Baker, *Am Acad Pediatrics* **1993**, *92*, 699.
[13] H. K. Ballaji, R. Correia, C. Liu, S. Korposh, B. R. Hayes-Gill, A. Musgrove, S. P. Morgan, *Sensors* **2021**, *21*, 6072.
[14] M. Mrgan, D. Rytter, M. Brabrand, *Emerg Med J* **2014**, *31*, 954.
[15] Y. Monteerarat, R. Limthongthang, P. Laohaprasitiporn, T. Vathana, *Eur J Trauma Emerg Surg* **2021**, *48*, 1.
[16] A. Pandey, B. M. John, *Med J Armed Forces India* **2013**, *69*, 97.
[17] H. Ait-Oufella, N. Bige, P. Y. Boelle, C. Pichereau, M. Alves, R. Bertinchamp, J. L. Baudel, A. Galbois, E. Maury, B. Guidet, *Intensive Care Med* **2014**, *40*, 958.
[18] H. Otieno, E. Were, I. Ahmed, E. Charo, A. Brent, K. Maitland, *Arch Dis Child* **2004**, *89*, 977.
[19] I. Shavit, R. Brant, C. Nijssen-Jordan, R. Galbraith, D. W. Johnson, *Pediatrics* **2006**, *118*, 2402.
[20] S. Fleming, P. Gill, C. Jones, J. A. Taylor, A. Van Den Bruel, C. Heneghan, N. Roberts, M. Thompson, *PLoS One* **2015**, *10*, e0138155.
[21] World Health Organization, *Dengue: guidelines for diagnosis, treatment, prevention, and control*, World Health Organization, Geneva, Switzerland **2009**.
[22] B. Yormaz, H. A. Cizmecioglu, M. H. Goktepe, N. Ahmadli, D. Ergun, B. Tulek, F. Kanat, A. Cizmecioglu, *Selcuk Tip Dergisi* **2021**, *3*, 224.
[23] K. Shinozaki, L. S. Jacobson, K. Saeki, N. Kobayashi, S. Weisner, J. M. Falotico, T. Li, J. Kim, J. W. Lampe, L. B. Becker, *Crit Care* **2019**, *23*, 157.

[24] B. Anderson, A. M. Kelly, D. Kerr, D. Jolley, *Hong Kong J Emerg Med* **2008**, *15*, 71.
[25] L. H. Brown, N. Heramba Prasad, T. W. Whitley, *Am J Emerg Med* **1994**, *12*, 46.
[26] R. T. John, J. Henricson, J. Junker, C. O. Jonson, G. E. Nilsson, D. Wilhelms, C. D. Anderson, *J Biophotonics* **2018**, *11*, e201700371.
[27] A. Matas, M. G. Sowa, V. Taylor, G. Taylor, B. J. Schattka, H. H. Mantsch, *Adv Skin Wound Care* **2001**, *14*, 180.
[28] J. Lewin, I. Maconochie, *Emerg Med J* **2008**, *25*, 325.
[29] T. P. Chang, G. Santillanes, I. Claudius, P. K. Pham, J. Koved, J. Cheyne, M. Gausche-Hill, A. H. Kaji, J. Saranya Srinivasan, J. Donofrio, C. Bir, *Prehosp Disaster Med* **2017**, *32*, 451.
[30] K. Shinozaki, L. S. Jacobson, K. Saeki, H. Hirahara, N. Kobayashi, S. Weisner, J. M. Falotico, T. Li, J. Kim, L. B. Becker, *J Intensive Care* **2019**, *7*, 52.
[31] E. Kerr, S. Coleman, T. M. McGinnity, A. Shepherd, IEEE Computer Society Conference on Computer Vision and Pattern Recognition Workshops (CVPRW), Salt Lake City, UT, USA, **2018**, p. 1372.
[32] Ç. Ahmet, T. Dilek, H. Selda, Y. Sema, *Konuralp tıp dergisi* **2022**, *14*, 114.
[33] R. T. John, J. Henricson, C. D. Anderson, D. B. Wilhelms, *Emerg Med J* **2019**, *36*, 465.
[34] S. L. Jacques, J. C. Ramella-Roman, K. Lee, *J Biomed Opt* **2002**, *7*, 329.
[35] W. Groner, J. W. Winkelman, A. G. Harris, G. J. Bouma, K. Messmer, R. G. Nadeau, C. Ince, G. J. Bouma, K. Messmer, R. G. Nadeau, *Nat Med* **1999**, *5*, 1209.
[36] I. Stockford, S. Morgan, *Opt Lett* **2003**, *28*, 114.
[37] B. Anderson, A. M. Kelly, D. Kerr, M. Clooney, D. Jolley, *Am J Emerg Med* **2008**, *26*, 62.
[38] M. Borovkova, A. Bykov, A. Popov, I. Meglinski, in *Optics InfoBase Conference Papers*, Vol. F142 (Eds: A. Amelink, S. K. Nadkarni), SPIE, Munich, Germany, **2019**, p. 25.
[39] J. M. Saavedra, G. D. Harris, S. Li, L. Finberg, *Am J Dis Child* **1991**, *145*, 296.
[40] P. E. Bickler, J. R. Feiner, J. W. Severinghaus, *Anesthesiology* **2005**, *102*, 715.
[41] T. Phan, R. Rowland, A. Ponticorvo, B. C. Le, R. H. Wilson, S. A. Sharif, G. T. Kennedy, N. P. Bernal, A. J. Durkin, *J Biomed Opt* **2021**, *26*, 026001-01.
[42] A. P. Popov, A. V. Bykov, I. V. Meglinski, *J Biomed Opt* **2017**, *22*, 1.
[43] H. R. Champion, W. J. Sacco, D. S. Hannan, R. L. Lepper, E. S. Atzinger, W. S. Copes, R. H. Prall, *Crit Care Med* **1980**, *8*, 201.
[44] R. Kawaguchi, T.-a. Nakada, T. Oshima, M. Shinozaki, T. Nakaguchi, H. Haneishi, S. Oda, *Crit Care* **2019**, *23*, 1.
[45] C. Liu, R. Correia, H. Ballaji, S. Korposh, B. Hayes-gill, S. Morgan, *Sensors* **2020**, *20*, 1388-01.
[46] V. V. Tuchin, D. Zhu, E. A. Genina, *Handbook of Tissue Optical Clearing: New Prospects in Optical Imaging*, CRC Press, Boca Raton **2022**.
[47] O. Yasufumi, N. Morimura, A. Shirasawa, H. Honzawa, Y. Oyama, S. Niida, T. Abe, S. Imaki, I. Takeuchi, *J Intensive Care* **2019**, *7*, 29.
[48] Y. Cho, S. J. Julier, N. Bianchi-Berthouze, *J Med Internet Res* **2019**, *6*, e10140-01.
[49] M. Jacquet-Lagrèze, N. Bouhamri, P. Portran, R. Schweizer, F. Baudin, M. Lilot, W. Fornier, J.-L. Fellahi, *Crit Care* **2019**, *23*, 281.

How to cite this article: R. P. d. S. Bachour, E. L. Dias, G. C. Cardoso, *J. Biophotonics* **2023**, *16*(11), e202300063. https://doi.org/10.1002/jbio.202300063